

CFD Simulation and Experimental Study of a New Elastic Blade Wave Energy Converter

Chongfei Sun¹, Jianzhong Shang¹, Zirong Luo¹, Xin Li^{2,*}, Zhongyue Lu¹ and Guoheng Wu¹

¹College of Intelligence Science and Technology, National University of Defense Technology, Changsha, 410073, China

²College of Electronic Engineering, National University of Defense Technology, Hefei, 230031, China

*Corresponding Author: Xin Li. Email: lixinkiller@126.com

Received: 30 January 2020; Accepted: 27 October 2020

Abstract: Small moving vehicles represent an important category of marine engineering tools and devices (equipment) typically used for ocean resource detection and maintenance of marine rights and interests. The lack of efficient power supply modes is one of the technical bottlenecks restricting the effective utilisation of this type of equipment. In this work, the performance characteristics of a new type of elastic-blade/wave-energy converter (EBWEC) and its core energy conversion component (named wave energy absorber) are comprehensively studied. In particular, computational fluid dynamics (CFD) simulations and experiments have been used to analyze the hydrodynamics and performance characteristics of the EBWEC. The pressure cloud diagrams relating to the surface of the elastic blade were obtained through two-way fluid-solid coupling simulations. The influence of blade thickness and relative speed on the performance characteristics of EBWEC was analyzed accordingly. A prototype of the EBWEC and its bucket test platform were also developed. The power characteristics of the EBWEC were analyzed and studied by using the blade thickness and motion cycle as control variables. The present research shows that the EBWEC can effectively overcome the performance disadvantages related to the transmission shaft torque load and power curve fluctuations of rigid blade wave energy converters (RBWEC).

Keywords: Elastic blade wave energy converter; structural design; energy conversion mechanism; computational fluid dynamics simulation; experiment; hydrodynamic characteristics

1 Introduction

The ocean is rich in mineral resources, fishery resources and renewable energy [1–4]. The exploitation of marine resources is of great significance for maintaining the stable development of the world economy. In order to strengthen the hard power and speech right in the field of ocean resource development, the traditional maritime powers have strengthened their technological research and development of marine engineering equipment [5–7]. Small low-power unmanned marine engineering equipment represented by unmanned surface/underwater vehicle is widely used in the fields of deep-sea exploration, marine communications, and unmanned operations [8,9].



This work is licensed under a Creative Commons Attribution 4.0 International License, which permits unrestricted use, distribution, and reproduction in any medium, provided the original work is properly cited.

Most of the above mentioned marine engineering equipment needs to move frequently to change their work place, and keep various types of instruments turned on without interruption. This puts forward higher requirements for its power supply [10,11]. Most of the current small marine engineering equipment use battery power technology at present. Limited by the electricity capacity and reliability of batteries equipped, it is difficult for marine engineering equipment to further improve the endurance capacity and operation intensity [12]. The sustainable power supply technology with high energy density is the fundamental guarantee to improve the endurance and work intensity of small marine engineering equipment.

Small marine engineering equipment is surrounded by ocean energy, and using ocean energy is expected to fundamentally solve the problem of power supply. There are still some problems in power generation stability of ocean energy. Due to its large reserves, renewable and pollution-free characteristics, ocean energy is still closely concerned and focused by global scientific research institutions and innovative enterprises [13–15]. In addition, ocean energy, as a kind of environmentally friendly renewable energy, has less impact on the surrounding ocean environment than other power supply methods [16]. The energy characteristics of wide wave energy distribution area and high energy flow density are conducive to the energy extraction device to obtain a larger amount of energy in a smaller equipment space, so as to realize the miniaturization of the power supply module. Combining the energy characteristics of different types of ocean energy and the offshore working mode of small marine engineering equipment, wave energy is one of the most suitable ocean energy for powering small marine engineering equipment.

However, the research focus of wave energy extraction technology is mainly on large wave energy converters (WEC) currently. The power generation of large WEC is huge, and most of them require large mechanical components such as mooring systems and damping plates, so the overall size of the WEC is relatively large compared to the wavelength of the wave [17,18]. The power requirement of small unmanned marine engineering equipment is relatively small and most of them work in the open sea. So it is difficult to directly apply the existing wave energy extraction technology to small marine engineering equipment. If WEC is used as a power supply module and integrated into the marine engineering equipment, its device size must not be too large [18].

At present, the small marine engineering equipment lacks efficient and reliable power supply mode, and the existing large WEC cannot be directly used as the power supply module of small marine engineering equipment. For this reason, the wave energy research group of National University of Defense Technology proposed and developed a small-scale WEC, of which the core energy conversion component is a wave energy absorber [19]. The new small-scale WEC performs well in simplifying structure and improving efficiency, and is expected to be integrated into small marine engineering equipment as a power supply module and improve its endurance and operation intensity.

The research team conducted a comprehensive and detailed study on the performance characteristics of the first-generation principle prototype, that is, the rigid blade wave energy converter (RBWEC). Due to the excessive fluctuations in output power and load on the transmission shaft of RBWEC, a second-generation principle prototype was developed, namely the elastic blade wave energy converter (EBWEC). The existing research work mainly focuses on the theoretical study of the absorption mechanism and performance characteristics [20]. This paper uses CFD simulation and experiment as the main research means to analyze the hydrodynamic, power and efficiency characteristics of the EBWEC, which lays the foundation for the subsequent engineering of the EBWEC. The new WEC provides a potential technical solution for solving the power supply problem of small marine engineering equipment.

2 Structural Design and Energy Conversion Mechanism

The overall structural design of the new EBWEC is shown in Fig. 1. EBWEC mainly consists of two parts: surface floating body and underwater wave energy absorber, which are connected by tether. The tether is mainly made of steel cable to bear the pulling force of the floating body on the wave energy

absorber. In addition, a spiral wire with a certain resistance to stretching and bending is integrated inside the steel cable, which is used to transmit electrical energy and control signals. The EBWEC is integrated as a power supply module into small marine engineering equipment, so the marine engineering equipment can be used as a surface floating body for the converter. When the small marine engineering equipment needs to replenish energy, it will stop sailing and release the wave energy absorber below the sea surface. The small marine engineering equipment provides wave energy absorber with the heave motion needed for power generation. The electrical energy generated by wave energy absorber can be transmitted back to small marine engineering equipment through tether. After the electrical power was replenished, the marine engineering equipment can recover the wave energy absorber.

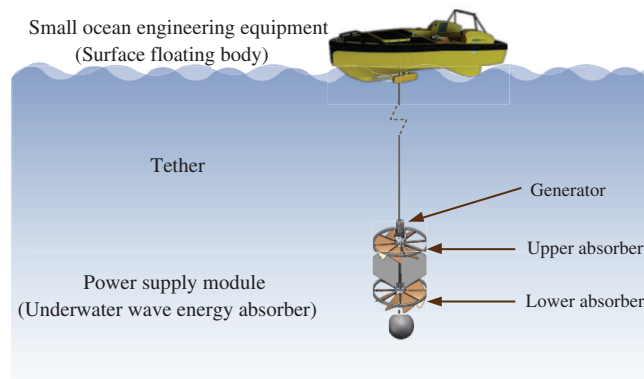


Figure 1: Overall structural design

Fig. 2 is the front view and section view of transmission structure design of wave energy absorber. The upper absorber is fixedly connected to the stator and shell of small generator. The lower absorber is fixedly connected to the transmission shaft at the center of absorber. The transmission shaft penetrates the central hole of the upper absorber, and is fixedly connected to the generator shaft and its rotor through a coupling. It can be seen that the reverse rotation movement of the generator stator and rotor comes from the upper and lower absorbers respectively. And the double absorbers provide the reverse rotation movement for the generator to generate electricity. The main function of the stabilizing fins is to prevent the underwater wave energy absorber from lateral deflection when it descends by its own gravity. The main function of the additional weight is to adjust the position of the center of gravity of the wave energy absorber according to different sea conditions to maintain the normal operation of the absorber. However, the stabilizing fins and the additional weight do not involve the transmission chain of the absorber.

The operation of the new EBWEC is based on the self-adaptive contra-rotation operation mechanism. Fig. 3 is a simplified diagram of the energy conversion mechanism of EBWEC. Its working process is as follows:

1. When the surface floating body rises, the underwater wave energy absorber is dragged by the tether and then rises. The upper surfaces of elastic blades of upper and lower absorbers are impacted by the water flow, and the blades are adaptively bent downward. The elastic blades generate bending stress due to elastic deformation, and then reach a state of force balance with the impact force of the water flow. The elastic blades finally stop bending downward and present a tilt state. The water body continues to impact the curved elastic blades and generate thrust, pushing the blades forward. As the elastic blades of the upper and lower absorbers are arranged in opposite directions, the upper absorber rotates counterclockwise, and the lower absorber rotates clockwise.

2. When the surface floating body is at the crest or trough of wave, the elastic blade theoretically will not produce elastic deformation, and cannot provide thrust for rotation of the absorber. Since the transient static state of the absorber at the crest and trough is short, this can minimize the stall time. And the inertia of the absorber itself makes it easy to keep rotating in the original direction.
3. When the surface floating body sinks, the underwater wave energy absorber sinks due to its own gravity. The principle of the reverse rotation movement of the upper and lower absorbers in the sinking state is similar to that in the rising state. Since the direction of the component force of the thrust of elastic blade has not changed, the rotation direction of the absorber in the sinking state is consistent with that in the rising state.

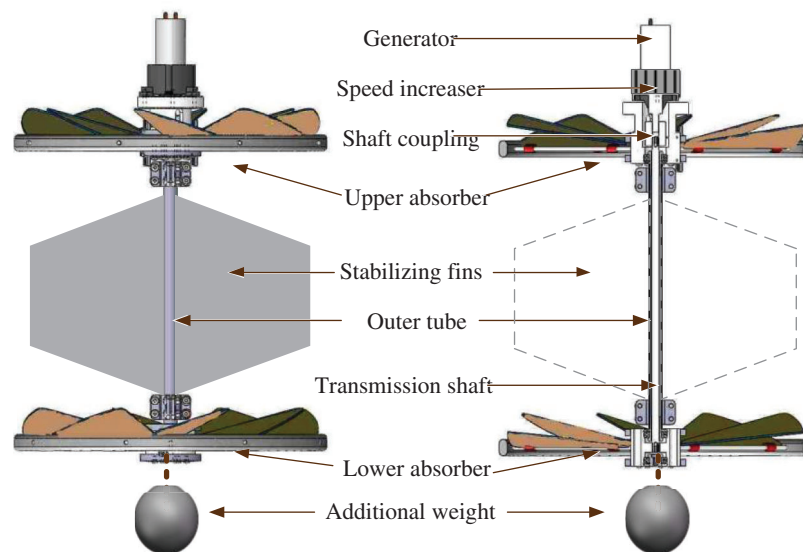


Figure 2: Transmission structure design

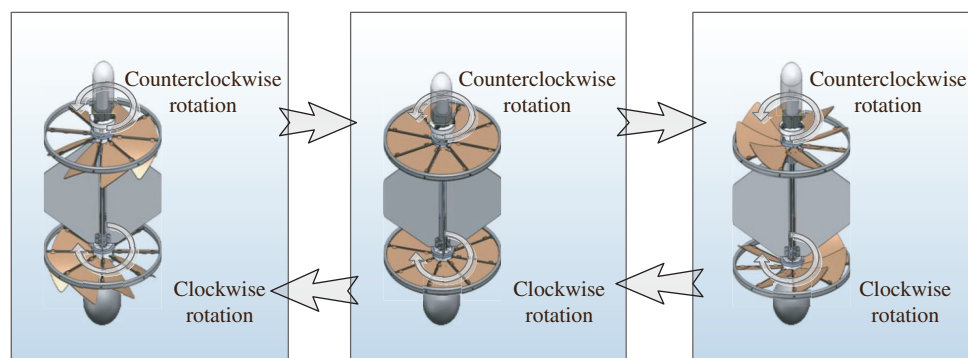


Figure 3: Schematic diagram of energy conversion mechanism

3 CFD Simulation Results and Discussions

There is a complex two-way fluid-structure coupling effect between the elastic blade of EBWEC and its surrounding flow field. The elastic blade is subject to bending deformation under the impact of water flow, and the continuous deformation of the blade surface changes the distribution of its surrounding flow field. The non-constant shape changes of the elastic blades make it difficult to accurately quantify the

performance characteristics and hydrodynamic characteristics of the absorber in the way of theoretical analysis. In view of the advantages of current computational fluid dynamics (CFD) technology in visualization of flow pattern distribution and quantification of physical parameter distribution [21], CFD simulation method was used to study the fluid-solid coupling characteristics between the elastic blade and the water flow and the mechanical characteristics of the blade surface.

3.1 Numerical Method and Grid Generation

The ANSYS Workbench was used to simulate the two-way fluid-structure interaction between the elastic blade and its surrounding flow field. The underlying principles is shown in Fig. 4. The Design Modeler module is used to preprocess the imported geometry files. The fluid computational domain and solid computational domain are divided respectively. Then the geometric models of the fluid computing domain and the solid computing domain are imported into the Fluent module and the Transient Structural module, respectively. The System Coupling module is used to couple and transfer the flow field data in the Fluent module and the structural data in the Transient Structural module, and the mechanical characteristics data of elastic blade are obtained through iterative calculation [22]. It should be noted that the numerical method is used to study the hydrodynamic characteristics (such as hydraulic power and efficiency) of the new elastic blade WEC, but it is difficult to directly measure the above physical quantities in the experiment. Therefore, in the previous study, our research group verified the rationality and accuracy of the numerical simulation method by comparing the changing trend of hydraulic power curve and electrical energy output power curve of the WEC [20].

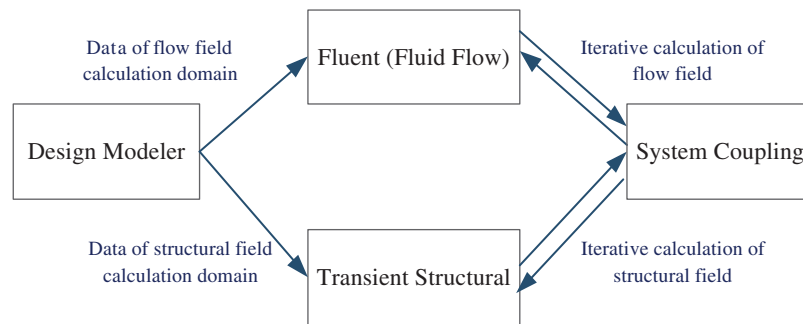


Figure 4: Underlying principles of two-way fluid-structure interaction

The unsteady-state Navier-Stokes equations in a conservative form were solved by the finite volume method in ANSYS Fluent. And the finite volume method is considered by many scholars to be the preferred numerical method for complex geometry in CFD analysis [23]. The mathematical conservative Navier-Stokes equations for mass and momentum can be expressed as follows [24]:

$$\frac{\partial \rho}{\partial t} + \nabla(\rho \vec{v}) = 0 \quad (1)$$

$$\frac{\partial}{\partial t}(\rho \vec{v}) + \nabla(\rho \vec{v} \vec{v}) = -\nabla p + \nabla(\vec{\tau}) + \rho \vec{g} \quad (2)$$

where ρ is the fluid density, t is the time variable, \vec{v} is the velocity vector, p is the pressure, and $\vec{\tau}$ is the stress vector, \vec{g} is the acceleration vector of gravity.

Eqs. (1) and (2) are general forms of governing equations applicable to both compressible and incompressible fluids. In the fluid structure coupling simulation in this work, the fluid density changes little and can be regarded as incompressible, that is, the ρ in the system of equations is set as a constant.

The pressure based solver has better computational applicability in low-speed incompressible flow. So the pressure-based solver was used to perform transient calculation of the two-way fluid-structure interaction of the blade. Since the governing equations are nonlinear and coupled to one another, the solution process involves iterations wherein the entire set of governing equations is solved repeatedly until the solution converges. The pressure-based solver uses a solution algorithm where the governing equations are solved sequentially [25]. According to the User's Guide of the fluid module, i.e., Fluent, the PISO (Pressure-Implicit with Splitting of Operators) separation algorithm has a good performance in the calculation of unsteady flow containing higher tilted grids [26]. Therefore, PISO was selected as the solution to the pressure-velocity coupling equation.

The SST k - ω model was selected as the turbulence model, which takes advantage of the calculation advantages of standard k - ω model in the boundary layer backpressure gradient region and k - ϵ model in free shear flow. The turbulence kinetic energy, k , and the specific dissipation rate, ω , can be obtained from the following transport equations [27]:

$$\frac{\partial}{\partial t}(\rho k) + \frac{\partial}{\partial x_i}(\rho k v_i) = \frac{\partial}{\partial x_j} \left(\Gamma_k \frac{\partial k}{\partial x_j} \right) + \tilde{G}_k - Y_k \quad (3)$$

$$\frac{\partial}{\partial t}(\rho \omega) + \frac{\partial}{\partial x_i}(\rho \omega v_i) = \frac{\partial}{\partial x_j} \left(\Gamma_\omega \frac{\partial \omega}{\partial x_j} \right) + G_\omega - Y_\omega + D_\omega \quad (4)$$

where \tilde{G}_k is the generation of turbulence kinetic energy due to mean velocity gradients. G_ω is the generation of ω . Γ_k and Γ_ω are the effective diffusivity of k and ω , respectively. Y_k and Y_ω are the dissipation of k and ω due to turbulence.

More detailed features make the shape of the fluid computing domain around EBWEC relatively complicated. The intensification of the interaction between the elastic blade and the surrounding flow field will also increase the distortion and the number of tetrahedral mesh. The elastic blades of the absorber are arranged in a circular array with central symmetry. The stress and deformation of different elastic blades are similar. Therefore, it is not necessary to perform numerical simulation on all elastic blades. Through performing fluid-structure interaction simulation on a single blade, the performance characteristics of the entire wave energy absorber can be obtained. This is in line with the research requirements for the performance characteristics of absorber at the beginning of study.

The main mathematical models and numerical methods required for fluid-structure coupling simulation are summarized in [Tab. 1](#).

Table 1: Main configuration of mathematical models and numerical methods

Item	Configuration
Solver	Pressure-based
Turbulence model	SST k - ω
Pressure-velocity coupling equation	PISO algorithm
Initialization method	Hybrid
Mesh division method	Tetrahedral mesh
Grid computing form	Dynamic meshing
Inlet boundary condition	Velocity inlet
Outlet boundary condition	Pressure outlet
Spatial Discretization	Second-Order Upwind

The main calculation parameters required for fluid-structure coupling simulation are summarized in [Tab. 2](#).

Table 2: Main parameters of simulation calculation

Item	Value
Blade density	7.82 kg/m ³
Elastic Modulus	2.1 × 10 ⁵ MPa
Poisson's ratio	0.28
Initial angle of attack	18.8°
Maximum relative speed	0.4962, 0.5686, 0.6824 m/s
Blade thickness	0.05, 0.10, 0.15, 0.20, 0.25 mm

The tetrahedral mesh with good applicability to the shape of the computational domain was selected. The quality and accuracy of mesh generation can be improved by orthogonality and aspect ratio subsequently. Dynamic meshing technology was used to simulate this kind of strong fluid-solid coupling situation where fluid-solid boundary changes continuously. In order to ensure that the accuracy and convergence of simulation results are not affected by grid generation, it is necessary to conduct grid refinement study [28,29]. The torque of a single absorber blade was selected as a physical variable to observe the influence of the number of grid points change on the calculation results, as shown in [Tab. 3](#).

Table 3: Mesh sensitivity analysis

No. of grid points (×10 ⁶)	Torque value (N·m)
0.3	0.2176
0.4	0.2409
0.5	0.2553
0.6	0.2524
0.7	0.2547
0.3	0.2176

Through the reasonable numerical configuration and parameter setting, the two-way fluid-structure coupling simulation calculation on a single elastic blade was carried out, and the power efficiency characteristics of the entire absorber were finally obtained. Taking the elastic blade with a relative speed of 0.5686 m/s and a blade thickness of 0.10 mm as an example, the pressure cloud diagram of the pressure side and suction side surfaces of the elastic blade were analyzed, as shown in [Fig. 5](#). When the elastic blade of wave energy absorber is impacted by the water flow, the forces on its pressure side and suction side are not the same. The pressure on the pressure side of the blade is mainly positive, while the pressure on the suction side is mainly negative. The pressure difference between the two surfaces of the blade forms the moment of the elastic blade to the absorber transmission shaft. Both the high-pressure and low-pressure areas of the blade are concentrated in the leading edge of the blade. That is, the high-pressure difference area of the blade is mainly concentrated near the blade fixing rod. The pressure difference on the blade surface gradually decreases along the chord line direction and approaches zero at the trailing edge.

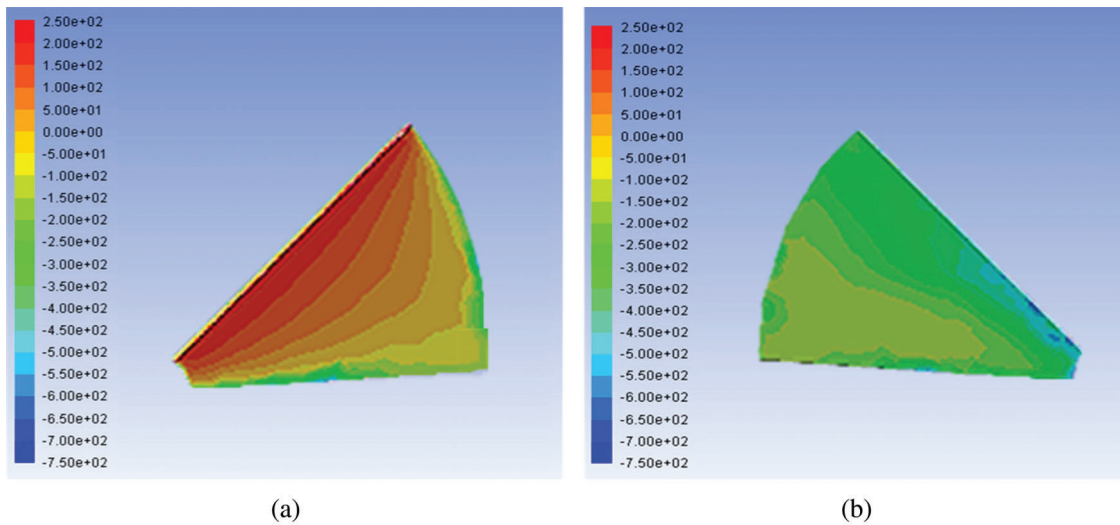


Figure 5: Pressure cloud diagram of elastic blade. (a) Pressure side, (b) Suction side

The change laws of mechanical output power and hydraulic efficiency of the wave energy absorber at three relative speeds selected in the simulation calculation are similar, as shown in Fig. 6. When the thickness of the elastic blade increases, the peak power of the absorber increases first and then decreases, and tends to be flat finally. The peak power of the absorber reached the highest value at the blade thickness of 0.10 mm. Because the input power of the absorber at the same relative speed is the same, the hydraulic efficiency change trend of the absorber is consistent with the mechanical output power. The highest output power of the absorber is 12.8 W, which is obtained when the blade thickness of the absorber is 0.10 mm and the relative speed is 0.6824 m/s; the highest hydraulic efficiency is 36.9%, which is obtained when the blade thickness is 0.10 mm and the relative speed is 0.5686 m/s.

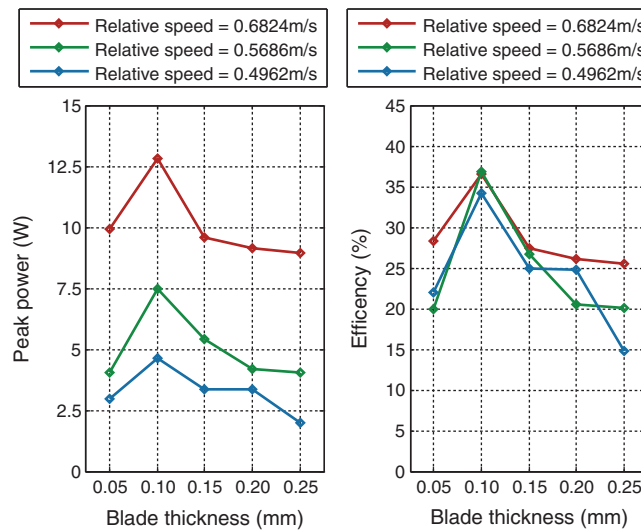


Figure 6: Effect of blade thickness on performance characteristics of absorber

4 Experimental Results and Discussions

The EBWEC prototype and bucket test platform were developed to verify the feasibility of the energy conversion mechanism of new EBWEC and analyze its hydrodynamic characteristics, as shown in Fig. 7. The structural composition of EBWEC is basically the same as that of RBWEC. The difference lies in the material and manufacturing process of blade and its related structures. The blades of the EBWEC prototype are made of 65 Mn elastic steel sheet, which is processed into fan-shaped blades by electric spark cutting, and the fixing holes are cut by laser drilling. The absorber frame made of epoxy fiberglass is used to replace the outer and inner rings of the absorber made of aluminum alloy, which can realize the lightweight and ensure the structural strength of the converter. The main structure of the EBWEC prototype adopts modular design, which is convenient for replacing parts to optimize the performance of the EBWEC and facilitate its subsequent maintenance.

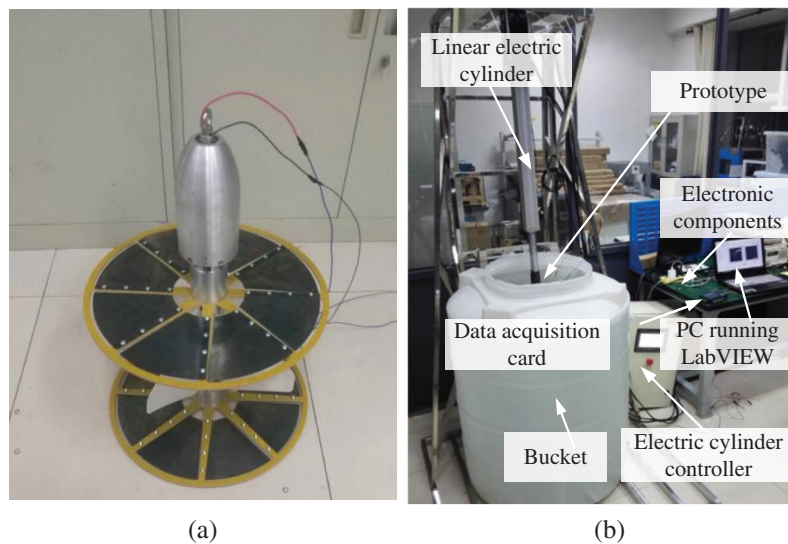


Figure 7: RBWEC prototype and its test platform. (a) EBWEC prototype, (b) Bucket test platform

The bucket-based test platform mainly includes a cylindrical test bucket, an electric cylinder that provides linear motion, an electric cylinder controller, a test PC running LabVIEW, a data acquisition card, and other necessary circuit components. The output shaft of the electric cylinder is fixedly connected to the RBWEC prototype for heave motion, and its motion amplitude and motion period can be accurately set by the corresponding controller. The current generated by the generator of the prototype is exported through the wires and flows through the load circuit. The data acquisition card collects the voltage and current data of the load circuit and imports it into the computer test system. The test system compiled by LabVIEW is used to calculate and process the imported data, and then output the power generation performance of the prototype in the form of graphics and data files. The main parameters of the bucket-based experiment are shown in Tab. 4.

4.1 Effect of Blade Thickness on EBWEC Performance

The performance characteristics of the new EBWEC are affected by many factors, especially the structure parameters of the converter itself and the external wave motion parameters. The research on the EBWEC is still in the initial stage at present. The blade thickness was selected as a typical variable of the structural parameters, and the motion period was selected as a typical variable of the wave motion parameters. The power characteristics of EBWEC prototype was tested quantitatively under the bucket test platform.

Table 4: Main parameters of the bucket-based experiments

Item	Values
Elastic blade material	65 Mn
Motion amplitude	150 mm
Motion period	1.5, 2.0, 2.5, 3.0, 3.5, 4.0 s
Blade thickness	0.05, 0.10, 0.15, 0.20, 0.25 mm

Fig. 8 shows the influence of blade thickness on the peak power and average power of the EBWEC. Three different motion periods were set in the experiments, with values of 2.0 s, 3.0 s, and 4.0 s. It can be seen from the figure that the peak power and average power curves of the converter increase sharply with the blade thickness first, and then decrease slowly. It can be found that the maximum power value of the converter is obtained when the blade thickness is 0.10 mm under different motion periods. Among them, the converter with a blade thickness of 0.10 mm achieves the highest power when the motion period was 2.0 s, the corresponding peak power and average power are 5.17 W and 3.05 W, respectively. Choosing a reasonable blade thickness is beneficial to produce the best deformation degree and the highest pressure difference of the elastic blade, thereby improving the power characteristics of the converter.

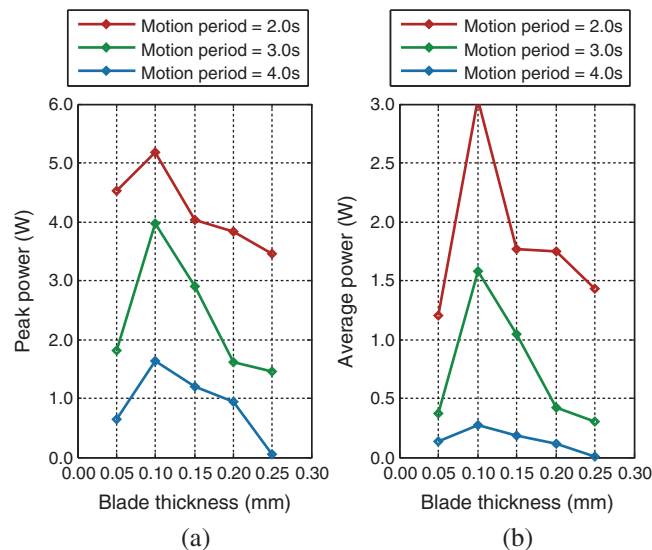


Figure 8: Effect of blade thickness on the power characteristics of the EBWEC. (a) Peak power curve, (b) Average power curve

4.2 Effect of Motion Period on EBWEC Performance

Fig. 9 shows the influence of the wave motion period on the peak power and average power of the EBWEC. Three different blade thicknesses were set in the experiments, with values of 0.05 mm, 0.15 mm, and 0.25 mm, respectively. It can be seen from the figure that the peak power and average power curves of different blade thicknesses decrease gradually with the increase of motion period. When the blade thickness of the converter is 0.05 mm and 0.15 mm, its peak power is relatively high, and the average power of the converter with the blade thickness of 0.15 mm is the highest. The EBWEC with a blade thickness of 0.05 mm achieved the highest peak power when the motion cycle was 1.5 s, i.e., 5.09 W; the EBWEC with a blade thickness of 0.15 mm achieves the highest average power when the

motion period was 1.5 s, i.e., 2.33 W. It can be seen from the change law in the figure that the smaller the motion period, the higher the power performance of EBWEC. That is, the EBWEC under high sea conditions generates higher power.

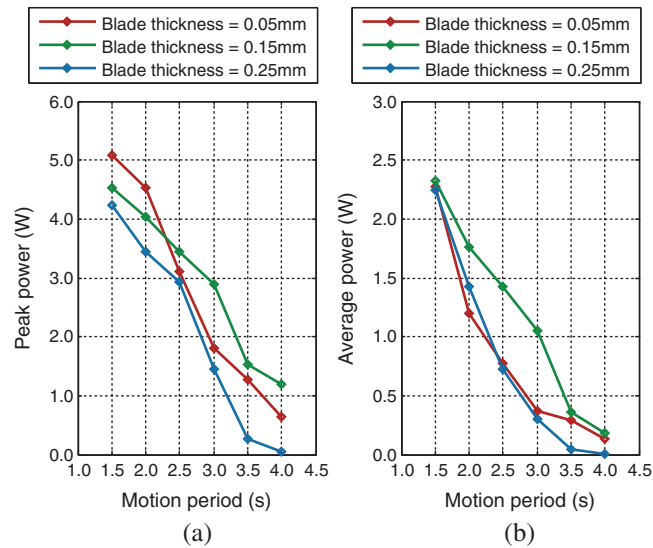


Figure 9: Effect of motion period on the power characteristics of the EBWEC. (a) Peak power curve, (b) Average power curve

As can be seen from Sections 4.1 and 4.2, the power characteristics of EBWEC are affected by the combined effect of blade thickness and wave motion cycle. And the influencing factors of converter performance characteristics are not completely independent, but related to each other.

5 Conclusions

The energy conversion mechanism and hydrodynamic characteristics of the new type of EBWEC were systematically studied in this paper. The CFD simulation results show that the wave energy absorber with a blade thickness of 0.10 mm can obtain a mechanical output power value of 12.8 W at a relative speed of 0.6824 m/s; the wave energy absorber with a blade thickness of 0.10 mm can achieve a hydraulic efficiency value of 36.9% at a relative speed of 0.5686 m/s. The Experimental results show that the EBWEC with a blade thickness of 0.10 mm can achieve the best power characteristics in most experimental environments. The EBWEC with a blade thickness of 0.10 mm achieved the highest power in the comparative experimental group when the motion period was 2.0 s, and its corresponding peak power and average power were 5.17 W and 3.05 W, respectively. The EBWEC effectively overcomes the performance disadvantage of large fluctuations in torque load and power curve during the operation, and improves its self-adaptive power generation ability under low sea conditions.

Funding Statement: This work was financially supported by the National Natural Science Foundation of China (Grant No. 51475465); the Hunan Provincial Innovation Foundation for Postgraduate (Grant No. CX2015B014).

Conflicts of Interest: The authors declare that they have no conflicts of interest to report regarding the present study.

References

1. Pelc, R., Fujita, R. M. (2002). Renewable energy from the ocean. *Marine Policy*, 26(6), 471–479. DOI 10.1016/S0308-597X(02)00045-3.
2. Zhang, P., Yang, L., Zhang, X. F., Tang, Y. (2010). The present status and prospect on exploitation of tuna and squid fishery resources in South China Sea. *South China Fisheries Science*, 6(1), 68–74.
3. Mero, J. L. (1965). *The mineral resources of the sea*. Amsterdam: Elsevier.
4. Astariz, S., Iglesias, G. (2015). The economics of wave energy: A review. *Renewable and Sustainable Energy Reviews*, 45, 397–408. DOI 10.1016/j.rser.2015.01.061.
5. Heo, J., Kim, J., Kwon, Y. J. (2017). Technology development of unmanned underwater vehicles (UUVs). *Journal of Computer and Communications*, 5(7), 28–35. DOI 10.4236/jcc.2017.57003.
6. Petersen, S., Krätschell, A., Augustin, N., Jamieson, J., Hein, J. R. et al. (2016). News from the seabed—Geological characteristics and resource potential of deep-sea mineral resources. *Marine Policy*, 70, 175–187. DOI 10.1016/j.marpol.2016.03.012.
7. Dincer, I. (2000). Renewable energy and sustainable development: A crucial review. *Renewable and Sustainable Energy Reviews*, 4(2), 157–175. DOI 10.1016/S1364-0321(99)00011-8.
8. López, A. M., Imiya, A., Pajdla, T., Álvarez, J. M. (2017). *Computer vision in vehicle technology: Land, sea & air*. John Wiley & Sons.
9. Seto, M. L. Ed. (2012). *Marine robot autonomy*. New York: Springer Science & Business Media.
10. Wang, X., Shang, J., Luo, Z., Tang, L., Zhang, X. et al. (2012). Reviews of power systems and environmental energy conversion for unmanned underwater vehicles. *Renewable and Sustainable Energy Reviews*, 16(4), 1958–1970. DOI 10.1016/j.rser.2011.12.016.
11. Henderson, E., Pantelakis, T., An, E. (2002). Energy systems for FAU AUVs. *Proceedings of the 2002 Workshop on Autonomous Underwater Vehicles*, Taipei, pp. 5–10.
12. Cai, Q., Brett, D. J. L., Browning, D., Brandon, N. P. (2010). A sizing-design methodology for hybrid fuel cell power systems and its application to an unmanned underwater vehicle. *Journal of Power Sources*, 195(19), 6559–6569. DOI 10.1016/j.jpowsour.2010.04.078.
13. Salter, S. H. (1974). Wave power. *Nature*, 249(5459), 720–724. DOI 10.1038/249720a0.
14. Regnier, E. (2007). Oil and energy price volatility. *Energy Economics*, 29(3), 405–427. DOI 10.1016/j.eneco.2005.11.003.
15. Lau, L. C., Lee, K. T., Mohamed, A. R. (2012). Global warming mitigation and renewable energy policy development from the Kyoto Protocol to the Copenhagen Accord—A comment. *Renewable and Sustainable Energy Reviews*, 16(7), 5280–5284. DOI 10.1016/j.rser.2012.04.006.
16. Mendez, A., Leo, T., Herreros, M. (2014). Current state of technology of fuel cell power systems for autonomous underwater vehicles. *Energies*, 7(7), 4676–4693. DOI 10.3390/en7074676.
17. Rusu, E., Onea, F. (2018). A review of the technologies for wave energy extraction. *Clean Energy*, 2(1), 10–19. DOI 10.1093/ce/zky003.
18. Norbach, A., Fjetland, K. B., Hestetun, G. V., Impelluso, T. J. (2018). Gyroscopic wave energy generator for fish farms and rigs. *ASME 2018 International Mechanical Engineering Congress and Exposition*. Pittsburgh: American Society of Mechanical Engineers Digital Collection.
19. Sun, C., Luo, Z., Shang, J., Lu, Z., Zhu, Y. et al. (2018). Design and numerical analysis of a novel counter-rotating self-adaptable wave energy converter based on CFD technology. *Energies*, 11(4), 694. DOI 10.3390/en11040694.
20. Sun, C., Shang, J., Luo, Z., Zhu, Y., Lu, Z. et al. (2019). Performance characteristics of a novel point absorber-type WEC based on counter-rotating self-adaptable movement mechanism. *Energy Sources, Part A: Recovery, Utilization, and Environmental Effects*, 42, 1–17. DOI 10.1080/15567036.2019.1632979.
21. Acharya, N., Kim, C. G., Thapa, B., Lee, Y. H. (2015). Numerical analysis and performance enhancement of a cross-flow hydro turbine. *Renewable Energy*, 80, 819–826. DOI 10.1016/j.renene.2015.01.064.
22. Zeiner-Gundersen, D. H. (2015). A novel flexible foil vertical axis turbine for river, ocean, and tidal applications. *Applied Energy*, 151, 60–66. DOI 10.1016/j.apenergy.2015.04.005.

23. Hirsch, C. (2007). *Numerical computation of internal and external flows: The fundamentals of computational fluid dynamics*. Oxford: Butterworth-Heinemann.
24. Ansys, Inc. (2009). ANSYS FLUENT 12.0 theory guide—1.2 continuity and momentum equations. <https://www.afs.enea.it/project/neptunius/docs/fluent/html/th/node11.htm>.
25. Ansys, Inc. (2009). ANSYS FLUENT 12.0 theory guide—18.1.1 pressure-based solver. <https://www.afs.enea.it/project/neptunius/docs/fluent/html/th/node361.htm>.
26. Ansys, Inc. (2009). ANSYS FLUENT 12.0 user's guide—26.3.1 choosing the pressure-velocity coupling method. <https://www.afs.enea.it/project/neptunius/docs/fluent/html/ug/node785.htm>.
27. Ansys, Inc. (2009). ANSYS FLUENT 12.0 theory guide—4.5.2 shear-stress transport (SST) k- ω model. <https://www.afs.enea.it/project/neptunius/docs/fluent/html/th/node67.htm>.
28. Fourie, L. F., Square, L. (2020). Determination of a safe distance for atomic hydrogen depositions in hot-wire chemical vapour deposition by means of CFD heat transfer simulations. *Fluid Dynamics & Materials Processing*, 16(2), 225–235. DOI 10.32604/fdmp.2020.08771.
29. Suri, Y., Islam, S. Z., Stephen, K., Donald, C., Thompson, M. et al. (2020). Numerical fluid flow modelling in multiple fractured porous reservoirs. *Fluid Dynamics & Materials Processing*, 16(2), 245–266. DOI 10.32604/fdmp.2020.06505.